

# High-channel-count, high-density microelectrode array for closed-loop investigation of neuronal networks

David Tsai, *Member, IEEE*, Esha John, Tarun Chari, Rafael Yuste and Kenneth Shepard, *Fellow, IEEE*

**Abstract** — We present a system for large-scale electrophysiological recording and stimulation of neural tissue with a planar topology. The recording system has 65,536 electrodes arranged in a 256 x 256 grid, with 25.5  $\mu\text{m}$  pitch, and covering an area approximately 42.6  $\text{mm}^2$ . The recording chain has 8.66  $\mu\text{V}$  rms input-referred noise over a 100 ~ 10k Hz bandwidth while providing up to 66 dB of voltage gain. When recording from all electrodes in the array, it is capable of 10-kHz sampling per electrode. All electrodes can also perform patterned electrical microstimulation. The system produces ~ 1 GB/s of data when recording from the full array. To handle, store, and perform nearly real-time analyses of this large data stream, we developed a framework based around Xilinx FPGAs, Intel x86 CPUs and the NVIDIA Streaming Multiprocessors to interface with the electrode array.

## I. INTRODUCTION

The functions of the mammalian central nervous system emerge from the orchestrated activities of a large number of neurons across space and time. To understand how this system performs computation, we need to observe the activities of large neuronal populations at high spatiotemporal resolution. Such information allows one to investigate how neighboring neurons operate both at a local scale and across large distance, elucidating the cooperative behaviors of small circuits and how these might give rise to emergent properties not achievable locally. Conventional electrophysiological tools (e.g. [1], [2], [3], [4], and [5]) have been able to accomplish either (1) localized but high-density recording (down to the scale of recording from all neurons within a small area) or (2) spatially extended recording with sparse sampling. What has been missing is the ability to do both simultaneously. In addition, because of sparse sampling, extracellular electrophysiological recording is typically blind to the number and locations of the neurons around the electrode [7], an instance of the blind source separation problem. Increasing the density of recording electrodes within a given spatial volume creates new abilities to distinguish the activity of different neurons [8], [9].

The ability to investigate neural networks is greatly enhanced if we can simultaneously perturb the constituent neurons in the network during recording. This should ideally occur at a spatial resolution and coverage comparable to the

recording. It should also occur with temporal resolutions comparable to spike timing. Finally, the amount of data generated during electrophysiological recordings scales with the number of electrodes. Therefore, tools attempting to achieve large-scale, high-resolution recordings of the nervous system need to address requirements for data throughput, storage, and real-time feedback.

We have developed a system ideally suited for large-scale investigations of neural networks with two-dimensional topologies, such as the retina, brain slices, and cultured neurons. The system consists of an active multielectrode array with 65,536 electrodes covering an area of approximate 42.6  $\text{mm}^2$  and with 25.5  $\mu\text{m}$  electrode pitch. When recording from the entire array, each electrode can be sampled at 10 kHz, thereby achieving true full-array coverage at physiologically relevant sampling rates. Each electrode can also be independently programmed to perform electrical microstimulation. We have built a heterogeneous computing platform using Xilinx FPGAs, Intel x86 CPUs, and NVIDIA SIMD streaming multiprocessors for handling and storing the recorded data, providing nearly real-time analyses capability, such as data filtering, spike detection, spike feature extraction, and sorting.

## II. RESULTS & DISCUSSION

### A. System Architecture

The active multielectrode array (MEA) circuit was fabricated in commercial 180-nm complementary metal-oxide-semiconductor (CMOS) process, the die photo of which is shown in Fig. 1B. The front-end consists of 65,536 electrodes, arranged in a 256 x 256 grid, for interfacing with the biological tissue. Each electrode has dimensions 14 x 14  $\mu\text{m}$  with a 25.5- $\mu\text{m}$  pitch between electrodes. This arrangement permits high-spatial-density sampling, up to the scale of having at least one electrode for each neuron, while maintaining extensive area coverage of up to 42.6  $\text{mm}^2$ .

Each electrode is capable of recording and stimulation. The MEA circuit architecture is summarized in Fig. 1A. The electrodes are coupled to the biological sample by means of a 2.5-pF blocking capacitor, which is incorporated into the electrode in post-processing steps described below. This capacitor in conjunction with a resistor, formed from a PFET operated in weak inversion, creates a user-tunable high-pass filter with corner frequency  $\leq 100$  Hz.

D. Tsai, T. Chari, and K. L. Shepard are with Electrical Engineering, Columbia University, NY, USA. D. Tsai and R. Yuste are with Biological Sciences, Columbia University, NY, USA. Correspondence: shepard@ee.columbia.edu.

This work is supported in part by the U.S. Army Research Laboratory and the U.S. Army Research Office under contract number W911NF-12-1-0594 to R. Yuste and K. L. Shepard, and a National Health & Medical Research Council of Australia CJ Martin Fellowship APP1054058 to D. Tsai.

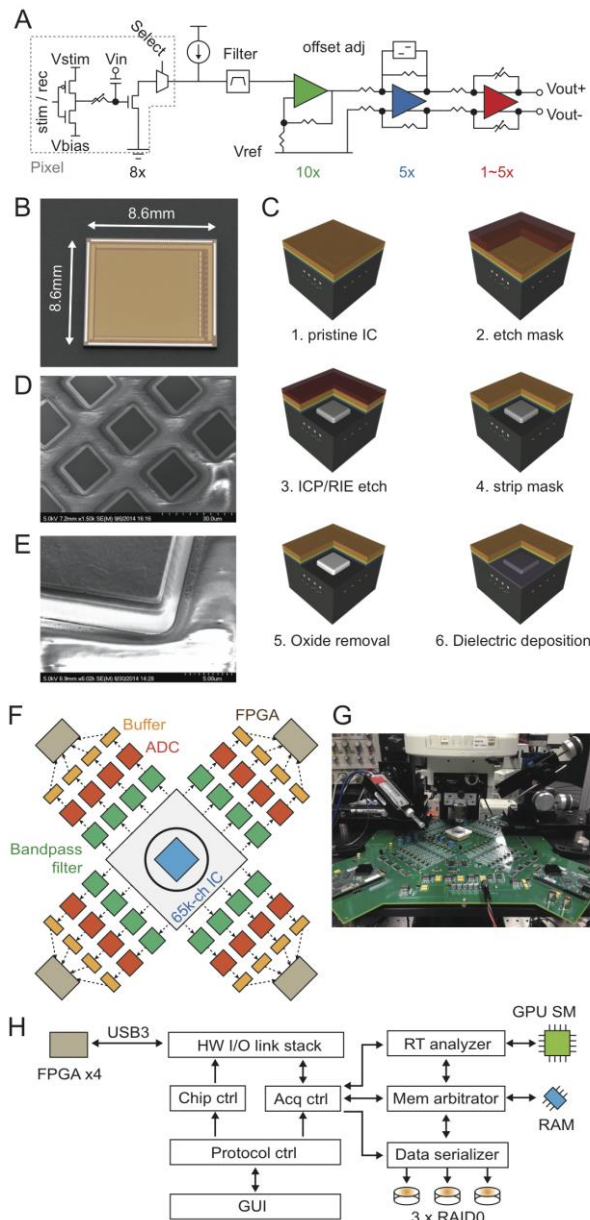


Figure 1: Multielectrode array (MEA) for large-scale, high-density investigations of neural networks. A. Simplified schematic of the stimulation and recording circuits. B. Die photo of unprocessed IC. C. Summary of in-house post-processing steps, to expose and prepare the electrodes for biological recordings. D. SEM image of the exposed electrode grid, prior to  $\text{HfO}_2$  deposition. E. High-magnification lateral view of one electrode, showing protrusion above the IC surface. F. Major component blocks of the custom circuit board for interfacing with the active MEA; signal digitization; and communication with a PC. G. Photo of the typical setup used in our experiments. H. Block diagram of major components in the acquisition system running on the PC.

To reduce inter-channel crosstalk and noise pickup by signal routing within the active MEA, a first-stage  $8\times$  amplification occurs with an electrode-level amplifier. Faithful recordings of small-amplitude ( $< 100 \mu\text{V}$  peak-to-peak) mammalian action potentials require low noise amplifiers with input-referred noise levels of less than  $10 \mu\text{V}$  rms over a  $100 \sim 10\text{k}$  Hz bandwidth. The first-level amplifier in the signal path dominates the MEA's overall noise

performance, which is, in turn, dominated by the flicker (or  $1/f$ ) noise of the input transistor. This device is made as large as possible within the allowable electrode area. As shown in Fig. 1A, the first-level amplifier consists of three transistors: a NFET, gate-coupled to the neural signal by means of the electrode-integrated blocking capacitor, and a transmission gate consisting of a NFET and PFET pair. The latter is used for multiplexing each pixel output into subsequent gain stages. The  $8\times$  amplification was chosen as a balance between higher gains, which improve overall noise performance requirements of subsequent amplifier stages, and lower gains, which limit the process-temperature-voltage (PVT) variations in dc bias levels across the array. The latter consideration is particularly important for this very simple first-stage amplifier design lacking feedback.

Signals from the 65,536 front-end amplifiers are multiplexed down to sixteen analog amplifier chains. These provide three additional stages of amplification providing at least 60 dB of additional gain. Each chain begins with a band-pass filter stage, with a user-adjustable high-pass corner frequency, nominally set to 100 Hz, and a low-pass corner frequency at 50 MHz. When sampling at 10 kHz per electrode while multiplexing the full array down to sixteen output lines, the signal path need a minimum bandwidth of 41 MHz to pass the resulting signals. The entire amplifier chain supports a 50-MHz bandwidth. The second stage is single ended, providing 20 dB of gain. The signal is then amplified by two subsequent fully differential amplifiers stages. A full-differential topology is chosen here to maximize common-mode rejection of noise arising from the digital switching of the multiplexing address lines. The last amplifier has programmable gain to allow adjustments for input signal amplitude variations across biological samples. The first full-differential opamp has a trimming circuit for eliminating dc offsets amplified by the preceding stages, avoiding saturation in the last amplifier stage. All three opamps use a folded cascode topology to maximize the input range for a 1.8-V supply voltage. The last-stage opamp contains a class AB stage to achieve rail-to-rail operation, allowing full use of the 1.8-V swing.

To provide real-time, closed-loop investigations with high spatiotemporal precision, each of the 65,536 electrodes can be independently programmed for microstimulation through the electrode blocking capacitor. This is achieved by configuring a register at each electrode to indicate whether a stimulating voltage will be applied during the next time interval of a 50-MHz clock. The stimulus voltage is adjustable to provide fine-grained control over microstimulation strength.

### B. Post processing

Following foundry processing, the diced integrated circuits (ICs) (Fig. 1B) are further processed in-house (Fig. 1C). The passivation stack (polyimide, silicon nitride and silicon dioxide) overlying the  $256 \times 256$  electrode region is removed by inductively coupled plasma / reactive ion etching (ICP/RIE) with  $\text{SF}_6/\text{O}_2$ . Regions where the passivation stack is to be preserved are covered by spin-coating a  $20\text{-}\mu\text{m}$  positive-tone photoresist prior to dry etching. Scanning electron microscopy shows successful exposure of the electrodes (Fig. 1D and 1E). The electrodes protrude above

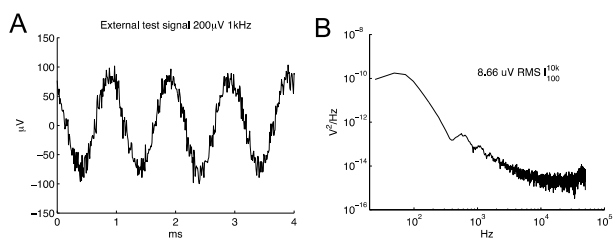


Figure 2: Electrical testing of the recording chain. A. Example recording when feeding a 200- $\mu\text{V}$  1-kHz sine wave into one electrode. B. Input-referred power spectral density of the recording system.

the IC surface (Fig. 1E). This is important for good contact between the neurons and the electrodes, providing for both high signal-to-noise ratio (SNR) recording and effective electrical stimulation. Complete removal of the passivation layers over the electrodes is further confirmed by energy dispersive x-ray spectrometry (EDX). To ensure rigorous control of the dielectric thickness and material composition on the electrode, the naturally occurring aluminum oxide on each aluminum electrode is stripped by argon plasma milling immediately prior to deposition of 12-nm of  $\text{HfO}_2$  with atomic layer deposition (ALD) at  $150^\circ\text{C}$ . This gives an electrode capacitance of 2.5 pF or  $\sim 0.013\text{ pF}/\mu\text{m}^2$ . Finally, each post-processed die is attached to a custom BGA package, wire-bonded, encapsulated with medical-grade epoxy, and affixed with a polycarbonate ring to serve as the perfusion chamber. These materials were chosen for their biocompatibility [10].

### C. Acquisition interface

The data acquisition system is built around a custom printed circuit board (PCB) and a high-end PC. The PCB contains active filters, analog-to-digital converters (ADCs), field-programmable gate arrays (FPGAs) (Fig. 1F) and additional supporting and testing circuitry. A Sallen-Key

band-pass filter with third order cut-on at 50 Hz and fifth order roll-off at 50 MHz conditions the MEA's full-differential analog outputs prior to digitization by a 12-bit ADC. The 50-MHz ADC clock is synchronized to the on-chip electrode-level 50-MHz sampling on the MEA. One FPGA captures the digitized signals from four ADCs and sends the data to a computer. High input impedance CMOS buffers located between the ADCs and the FPGAs isolate analog and digital signals and supplies on the PCB.

The four FPGAs are independently clocked and spatially separate (although equidistant from the MEA by design). A board-level clock distribution tree and within-FPGA dynamic clock phase adjustment circuits ensure correct operational timing across the otherwise asynchronous system components. When sampling all 65,536 MEA electrodes at 10 kHz with 12-bit resolution, the system generates approximately 1 GB/s of data. This necessitates a high bandwidth link between the PCB and the controlling computer. Furthermore, low transmission latency is essential to prevent overflowing the 128 MB high-speed DDR3 RAM adjacent to each FPGA. Each of the four FPGAs utilizes an independent  $\sim 350\text{ MB/s}$  USB3 interface to the controlling PC. The custom PCB, arranged in a typical experimental configuration for recording while imaging under the microscope, is shown in Fig 1G.

### D. Real-time storage & analyses

At the PC (Fig. 1H) we employ a heterogeneous computing architecture including both Intel x86 hardware and NVIDIA streaming multiprocessors to performing near real-time analyses on the incoming data. At the bottom of the hierarchy, a driver stack encapsulates bidirectional I/O transactions through USB3. On top of this, a library abstracts chip control and acquisition-related operations. Data serialization routines, running as independent threads, stride incoming data from the four FPGAs across multiple SSD hard drives in RAID0 configuration to maximize throughput.

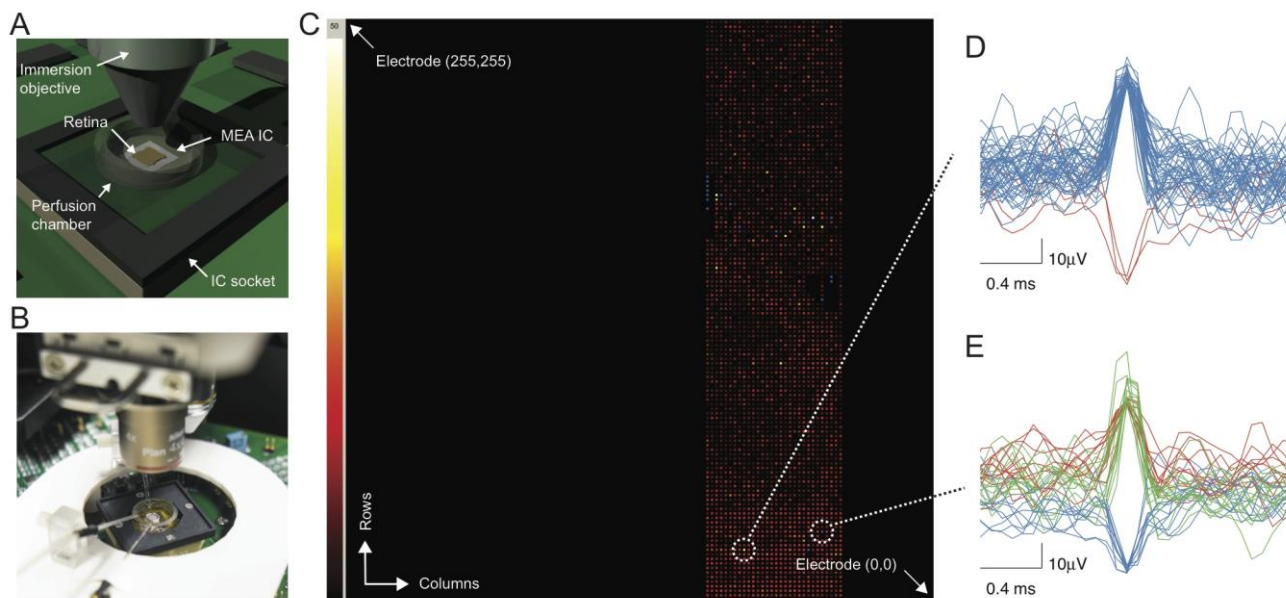


Figure 3: Spike recordings in mice retina. A. Our setup for recording spikes from mice retina using the MEA. B. Photo of a retina in the packaged MEA. C. Heat map illustrating the number of detected spikes when recording from a subset of the electrodes. The color scale denotes event count, which is capped to 50 ( $> 50$  events, blue). D and E. detected spikes at two electrodes. The putative units were spike sorted and distinguished by color.

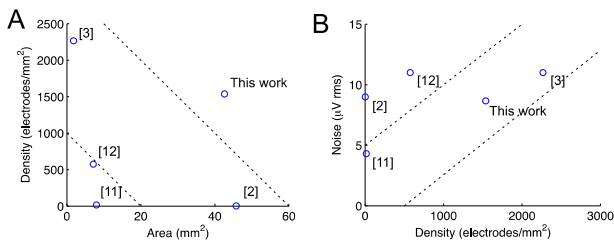


Figure 4: Comparison to other active MEAs.

This also prevents the order-of-magnitude-slower (compared to RAM access) disk-access time from stalling the rest of the system. Together these strategies allow us to store all data from all electrodes in real-time, for subsequent lossless data recall.

In order to perform real-time analyses (i.e. signal filtering, spike detection, feature extraction, and spike sorting), we stream the digitized signals to an NVIDIA Graphical Processing Unit (GPU) attached to the PC via a high-bandwidth 16-GB/s PCIe16x lane. We optimize the GPU routines for the SIMD architecture by maximizing core occupancy, minimizing code execution path branching, reducing GPU memory access, and maximizing coalesced memory fetches. Furthermore, we use a double-buffer swapping strategy for transferring data between the x86 host CPU and NVIDIA device GPU to increase execution parallelism. To manage scarce memory resources, we implemented a memory arbitrator to automatically garbage-collect data memory no longer referenced in the system at the earliest possible opportunity. Finally, an experimental protocol control layer, wrapped by a graphical user interface, presents a simple interface for interacting with the system during biological experiments.

#### E. Electrical testing

Two of the 65,536-electrodes were routed out to bond pads at the die perimeter. These electrodes allow us to verify and characterize IC functionality and to verify all the signal-processing hardware and software using known test signals. Fig. 2A shows the recording of a 200- $\mu$ V 1-kHz sine wave applied to one of the test electrodes. The small test signal, with amplitude comparable to those of typical mammalian neuronal spikes, is easily discernable from the noise.

An example of measured input-referred power spectral density plot is shown in Fig 2B. The recording chain has an integrated noise of 8.66  $\mu$ V rms over the 100 ~ 10k Hz bandwidth.

#### F. Biological recordings

To validate the recording capability of the system, a retina from a mature (> P30) C57BL6 mouse was isolated and placed flat on the MEA electrodes (Fig 3A). During the recording session the retina was kept alive by perfusing the imaging chamber with Ames Medium, supplemented with NaHCO<sub>3</sub> at 1.9 g/L, saturated with 95% O<sub>2</sub> and 5% CO<sub>2</sub>, heated to 34.5 °C, and at a rate of ~ 4 mL/min. Fig. 3B shows a photo from one experiment, with a piece of retina in the imaging chamber, and the perfusion ports attached. The MEA and the supporting circuit board were placed under a fixed-stage electrophysiology microscope. The experimental

procedures involving animal models described in this paper were approved by the Columbia University Institutional Animal Care and Ethics Committee. Fig. 3C shows a map of detected spiking events during a 30-s recording of a mouse retina. The MEA was configured to record from an area of 1.53 mm by 6.53 mm over the electrode grid. The bottom-right corner and top-left corner of the map correspond to the electrodes at location (0, 0) and (255, 255) in the grid, respectively. The colors represent the number of spikes detected ( $\geq 4.3$  standard deviations above baseline). Figs. 3D and 3E illustrate the actual signals from two electrodes. The waveform features were extracted by singular value decomposition. We then sorted all spikes from the putative neurons (distinguished by color in Fig. 2D and 2E) using the Expectation Maximization algorithm with a Gaussian mixture model over of first three principal components.

### III. CONCLUSION

We have developed an active multielectrode array for large-scale recording and near real-time analyses of neural activities, with single-cell resolution at electrode densities exceeding 1537 electrodes per mm<sup>2</sup> over an area exceeding 42.6 cm<sup>2</sup> (Fig. 4). The system is demonstrated here using the mouse retina. Additional applications areas include brain slices and cultured neurons.

### REFERENCES

- [1] A. M. Litke, E. J. Chichilnisky, W. Dabrowski, A. A. Grillo, P. Grybos, S. Kachiguine, M. Rahman and G. Taylor, "Large-scale imaging of retinal output activity," *Nuclear Instruments & Methods in Physics Research, Section A*, vol. 501, pp. 298-307, 2003.
- [2] U. Frey, U. Egert, F. Heer, S. Hafizovic and A. Hierlemann, "Microelectronic system for high-resolution mapping of extracellular electric fields applied to brain slices," *Biosensors and Bioelectronics*, vol. 24, pp. 2191-2198, 2009.
- [3] L. Berdondini, K. Imfeld, A. Maccione, M. Tedesco, S. Neukom, M. Koudelka-Hepb and S. Martinoia, "Active pixel sensor array for high spatio-temporal resolution electrophysiological recordings from single cell to large scale neuronal networks," *Lab on a chip*, vol. 9, pp. 2644-2651, 2009.
- [4] G. Buzsáki, "Large-scale recording of neuronal ensembles," *Nature Neuroscience*, vol. 7, pp 446-451, 2004.
- [5] R. A. Blum, J. D. Ross, E A. Brown and S. P. DeWeerth, "An Integrated System for Simultaneous, Multichannel Neuronal Stimulation and Recording," *IEEE Transactions on Circuits and Systems*, vol. 54, pp. 2608-2618, 2007.
- [6] Multichannel Systems, AG <http://www.multichannelsystems.com/>.
- [7] G. Buzsáki, "The origin of extracellular fields and currents - EEG, ECoG, LFP and spikes," *Nature Neuroscience*, vol. 13, pp. 407-420, 2012.
- [8] M. S. Lewicki, "A review of methods for spike sorting: the detection and classification of neural action potentials," *Network*, vol. 9, pp. R53-R78, 1998.
- [9] R. Quiñero, "What is the real shape of extracellular spikes?" *Journal of Neuroscience Methods*, vol. 177, pp 194-198, 2009.
- [10] C. Hassler, T. Boretius and T. Stieglitz, "Polymers for Neural Implants," *Polymer Physics*, vol. 49, pp. 18-33, 2011.
- [11] F. Heer, S. Hafizovic, W. Franks, T. Ugniwenko, A. Blau, C. Ziegler and A. Hierlemann, "CMOS microelectrode array for bidirectional interaction with neuronal networks," *Proceedings of ESSCIRC*, 2005.
- [12] K. Imfeld, S. Neukom, A. Maccione, Y. Bornat, S. Martinoia, P. Farine, Koudelka-Hepb and L. Berdondini, "Large-scale, high-resolution data acquisition system for extracellular recording of electrophysiological activity," *IEEE Transactions on Biomedical Engineering*, vol. 55, pp. 2064-2072, 2008